Properties of radiative charge transfer in heterogeneous noble-gas clusters

Xaver Holzapfel,[1] Tsveta Miteva,[2,*] Nicolas Sisourat,[2] Alexander Schrodt,[1] Lutz Marder,[1] Dana Bloß,[1] Christian Ozga,[1] Catmarna Küstner-Wetekam,[1] Arno Ehresmann,[1] André Knie,[1] and Andreas Hans[1,†]

[1]*Universität Kassel, Institut für Physik und CINSaT, Heinrich-Plett-Str. 40, D-34132 Kassel, Germany*

[2]*Laboratoire de Chimie Physique–Matière et Rayonnement UMR7614, CNRS/Sorbonne Université, 4 Place Jussieu, Tour 43/44, F-75252 Paris Cedex 05, France*

(Received 1 October 2021; revised 22 January 2022; accepted 24 January 2022; published 22 February 2022)

Radiative charge transfer (RCT) from cationic to neutral atoms is a fundamental and frequently occurring process in ion-neutral collisions and in van der Waals clusters. In contrast to collisions with only two collision partners, RCT in clusters is more involved as it may depend on the cluster size, the cluster stoichiometry, and the local arrangement of atoms in the cluster. Here, we present a systematic investigation of an RCT photon spectrum as a function of cluster size, stoichometry, and local atom arrangement. For this purpose, we utilize RCT in heterogeneous NeKr and NeXe clusters after Ne $2p$ photoionization. Our results confirm that Ne dimer ions form prior to RCT if enough Ne is available and we observe that different features dominate the photon spectrum depending on the cluster production parameters. Additionally, we find that the lifetime of the radiative decay is sensitive to the cluster stoichiometry, which we explain and interpret by theoretical calculations on the RCT decay width for different local geometric structures of the involved atoms. We conclude that RCT properties such as photon spectrum and lifetime in turn exhibit information on the mean size and stoichiometry of a cluster jet and the arrangement of the involved atoms.

DOI: 10.1103/PhysRevA.105.022815

I. INTRODUCTION

The role of interatomic processes in the decay of electronically excited van der Waals clusters has been studied intensely throughout the past decades, since it had been predicted in 1997 that even such weak bonds may completely change the decay route of excited atoms or molecules [1]. In the following years a large family of interatomic energy and charge transfer mechanisms has been identified [2–4].

Experimentally, coincidence experiments on photoexcited or -ionized dimers often enable insight of striking clarity [4]. The coincident detection of photoelectrons, secondary electrons, and the resulting ions allows the reconstruction of single and/or cascade decay mechanisms of electronically excited states [5]. This approach, however, becomes challenging for clusters of increasing size or for investigations on bulk matter. Scattered electrons and ions and evaporating neutrals hinder the full energetic reconstruction of the addressed initial process. Furthermore, systematic investigations on property changes of certain processes with cluster size are absolutely nontrivial. Experiments on size-selected neutral clusters, therefore, have only scarcely been performed so far [6]. Supersonic expansion, which is predominantly used to create van der Waals clusters, inherently produces a size distribution of clusters [7] with mean cluster size $\langle N \rangle$, the distribution of which may indeed be of width $\langle N \rangle$ [8,9]. Nevertheless, it is possible to investigate large clusters, considering that the experimental observables are averaged over a larger cluster size distribution. In many cases conclusions can still be drawn by investigating cluster jets of different mean cluster size $\langle N \rangle$.

Recently, we reported the experimental observation of a special member of the family of interatomic charge or energy transfer processes: the radiative charge transfer (RCT) in heterogeneous NeKr clusters [10]. Remarkably, this mechanism enables the electronic decay of singly valence ionized ground-state ions. In earlier experiments, a closely related process had been investigated in detail, in which an electron from the neutral environment partially neutralizes the charge state of a dication [11–13]. While in the latter case it is obvious that charge transfer minimizes the energy by lowering the Coulomb repulsion, in the singly charged case this is only possible in a heterogeneous environment.

In the particular example of heterogeneous NeKr clusters, the system's energy is minimized if a valence $4p$ electron from a Kr atom fills the vacancy in the Ne $2p$ valence shell. The released energy is emitted as a photon in the ultraviolet spectral range [10]. A detailed investigation of the RCT photon spectrum and the calculation of the Ne_2^+ potential-energy curve suggested nuclear dynamics to be relevant prior to the RCT. Before the Kr $4p$ electron is transferred, the ionized Ne atom forms Ne_2^+ with a neighboring Ne atom. In contrast, the creation of $(NeKr)^+$ was not observed, which can be understood by the much higher binding energy of Ne_2^+ compared to $(NeKr)^+$ [10,14].

A similar, yet different RCT process has already been observed earlier in high-pressure gas cell experiments using discharge excitation [15]. The RCT photon spectrum observed

*tsveta.miteva@upmc.fr
†hans@physik.uni-kassel.de

in this experiment differs significantly from that observed in the experiment with large heterogeneous clusters with the main contributions originating from NeKr dimers. Obviously, the Ne_2^+ formation is only possible in the large clusters and not in NeKr dimers.

It is now an intriguing question whether and how the RCT spectrum changes if the conditions of the supersonic expansion, which determine the stoichiometry of the clusters, are changed such that the amount of Ne atoms is decreased to gradually suppress Ne_2^+ formation and support the formation of NeKr dimers. In other words, does the RCT photon spectrum contain information on the stoichiometry of the heterogeneous clusters and the dynamics happening after photoionization and prior to RCT?

In the present work, we first corroborate our model of Ne_2^+ formation prior to RCT by substituting Kr by Xe and identifying a spin-orbit split doublet in the RCT photon spectrum. Subsequently, we investigate the RCT photon spectra and lifetimes for NeKr clusters of different sizes and stoichiometries.

II. EXPERIMENTS

To elucidate the properties of RCT for different cluster stoichiometries, several complementary experiments were performed at the synchrotron facility BESSY II (Helmholtz-Zentrum Berlin) at the UE112 PGM-1 and U125-NIM beamlines [16]. The experimental setup of the main experiments on dispersed photon spectroscopy has been described in detail in previous works [10,17]. Briefly, a mixture of 98.8% Ne and 1.2% Kr was expanded through a conical copper nozzle into the vacuum and clusters formed in the resulting supersonic expansion. We used nozzles with a full opening angle of 30° and diameters of 40 μm and 60 μm. A skimmer of 1.5 mm diameter separated the expansion and interaction chambers. In the interaction chamber, the cluster jet was crossed with linearly polarized monochromatic synchrotron radiation. Subsequently RCT photons are emitted, which were measured using dispersed photon spectroscopy [17,18].

The 1 m normal incidence spectrometer, used for the dispersed photon detection, was equipped with a 1 mm entrance slit, a grating with 600 lines per mm, and a position sensitive single-photon detector with a CsTe photocathode and a MgF_2 window, sensitive in the spectral range from 120 nm to 300 nm [17].

Dispersed luminescence spectra were measured at fixed exciting-photon energies above the first ionization threshold of atomic Ne I at 21.56 eV [20]. Additionally, the excitation energy was varied stepwise between 19 eV and 24 eV, and dispersed emission functions of NeKr clusters were recorded. Expansion conditions for the different measured spectra are given in Table I. We also list the mean cluster sizes which would result from expansion of a *homogeneous* gas according to commonly used scaling laws [19]. We are not aware of any work reporting on a procedure to determine the size and stoichiometry of heterogeneous NeKr clusters produced by coexpansion of a gas mixture. Because of a lacking model to estimate the cluster stochiometry accurately, we ensured proper cluster conditions by measuring other spectroscopic characteristics with the present conditions. The exciting-photon energy was also scanned stepwise across the Ne $2s \rightarrow np$ resonances in the energy range 45–49 eV, at which characteristic photon emission due to resonant interatomic Coulombic decay (rICD) can be observed [21]. Through a comparison of cluster specific and atomic features we confirmed during the experiment that we changed the parameters of the cluster production such that we indeed move from larger to smaller clusters and from high to low amount of condensed Ne [22]. Another, independent, confirmation is the observation of a slightly shifted onset of $2p$ photoionization, which is in line with the above considerations and will be discussed in more detail below. When comparing the results from empirical scaling laws for homogeneous clusters with our experimental observations, we found that, according to the scaling laws, the calculated cluster sizes of Fig. 2(c) contradict the experiment (see also Sec. III). This contradiction cannot fully be resolved with the present data. We therefore conclude that either the scaling laws are significantly inaccurate for the production of heterogeneous clusters or the documented experimental parameters are faulty. The latter can occasionally happen if, for example, the nozzle is partially blocked by condensing gas or impurities. We emphasize, however, that this fact does not influence our qualitative conclusions, since proper conditions were monitored by spectroscopic measurements throughout the experiment.

TABLE I. Experimental conditions used in the present experiments. *Homogeneous* cluster sizes for Kr and Ne are calculated according to Ref. [19] from the corresponding expansion conditions. All jets are expanded with a 1.2% mixture of Kr in Ne. Measurements presented in Fig. 2 were acquired at beamline UE112 PGM-1 and the spectra in Fig. 3 and Fig. 5 at beamline U125-NIM. The exciting-photon bandwidth ΔE is given in the last column.

	T, d, p_0 (K), (μm), (bar)	$\langle N\rangle_{Kr}, \langle N\rangle_{Ne}$ (atoms)	ΔE (meV)
Fig. 2(a)	120, 40, 3.26	2380, 16	15
Fig. 2(b)	156, 40, 4.00	1160, 8	29
Fig. 2(c)[a]	144, 60, 2.78	1560, 11	57
Fig. 3	90, 60, 0.70	900, 24	50
Fig. 5	140, 40, 3.50	1430, 10	50

[a]The calculated sizes of homogeneous clusters contradict the experimental observations in Fig. 2(c). These parameters should, therefore, be interpreted with caution (see text).

While the main experiment on the emission spectra of NeKr was performed at the UE112 PGM-1 beamline, the experiment on NeXe was carried out using the identical setup at the U125-2 10m NIM beamline. Here, the expansion conditions were 121 K and 6 bar using the 40 μm nozzle. The reference spectrum of homogeneous Xe clusters was taken at 190 K, 3.5 bar, and 40 μm nozzle. Also a cross-check NeKr spectrum and the emission function of the pure Kr features were taken at this beamline (see Sec. III and Table I).

Both the dispersed emission spectra and emission functions cannot be compared on an absolute intensity scale because of the unknown target density and composition. For better presentability the emission spectra have been normalized to one in their maximum. The emission functions have been normalized to the photon flux and scaled to coincide at 21.56 eV for easier comparison.

The experiments on emission spectra were performed in the multibunch hybrid operation mode of the storage ring. This operation mode offers high exciting-photon flux, which is beneficial for the emission spectra acquisition. However, it is in general not practical to determine radiative lifetimes, because the temporal spacing between consecutive exciting-photon pulses is too short. Experiments on the radiative lifetime, hence, need to be performed in single bunch operation mode, which provides 800 ns spacing between consecutive pulses, but only about 5% of the photon flux of multibunch hybrid mode. Consequently, emission spectra and lifetimes practically cannot be obtained in the same experiment. We therefore reanalyzed the data of our earlier experiment on RCT, performed in single bunch mode, and determined the lifetimes for two different expansion conditions (see Sec. III D). For experimental details we refer to Ref. [10].

III. RESULTS AND DISCUSSION

A. Emission spectra of NeXe

In our previous work, we suggested the formation of Ne_2^+ in the heterogeneous clusters prior to RCT [10]. Only the nuclear dynamics and subsequent charge transfer from one Kr atom to Ne_2^+ can explain the observed RCT photon spectrum. The central emission wavelength may then be determined by subtraction of the Kr $4p$ binding energy from the energy difference of the Ne_2^+ and Ne_2 potential-energy curves at the equilibrium internuclear distance of Ne_2^+. The resulting value of 4.6 eV (270 nm) is in good agreement with the experimental spectrum, which is broad but shows a pronounced maximum at about 265 nm.

In this estimate only the spectral feature resulting from charge transfer from the Kr $4p_{3/2}$ level is considered. In Kr the $4p_{3/2}/4p_{1/2}$ spin-orbit splitting is about 0.6 eV. In addition to the observed feature, a second maximum at 0.6 eV lower energy (4.0 eV = 310 nm) is thus expected. Due to the rapidly dropping quantum efficiency of the used photon detector with CsTe photocathode [17] no reliable conclusion could be drawn from the NeKr spectra for the $4p_{1/2}$ transition with lower emission energy. We therefore performed an analogous experiment on NeXe clusters. In Xe, the $5p_{3/2}$ to $5p_{1/2}$ spin-orbit splitting is 1.3 eV and, importantly, the $5p$ binding energy is about 1.9 eV lower than that of the Kr $4p$ level. If the model of Ne_2^+ formation is correct, we expect two features to be observed in the RCT photon emission spectrum of NeXe clusters, separated by 1.3 eV and shifted by 1.9 eV compared to the NeKr case, i.e., at approximately 6.5 eV (191 nm) and 5.2 eV (238 nm).

To exclude contributions from pure Xe clusters, the UV photon emission spectrum of homogeneous Xe clusters, excited by photons of 21.5 eV energy, is shown in Fig. 1(a). Three overlapping features can be identified, all of which have been already assigned to emission from Xe_2^* at 165 nm and 176 nm (M_1, M_2) and $(Xe_4^+)^*$ at 188 nm [23,24]. At the present exciting-photon energy, all these features can be induced by photoelectron impact excitation [25]. Because of the low Xe content in the mixture used for production of heterogeneous clusters, none of the features is observed in the respective emission spectrum of heterogeneous NeXe clusters; see Fig. 1(b). Instead, two pronounced maxima (labeled A and B) appear around 193 nm and 240 nm, matching well with the expected emission wavelengths for RCT from the $5p_{3/2}$ and $5p_{1/2}$ levels of Xe to Ne_2^+ and confirming the picture of Ne_2^+ formation prior to RCT.

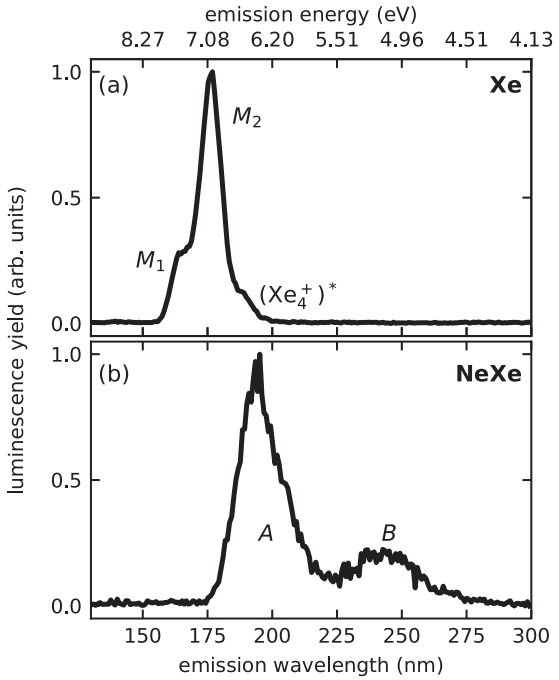

FIG. 1. Dispersed emission spectra of homogeneous Xe clusters (a) and heterogeneous NeXe clusters (b) for an exciting-photon energy of 21.5 eV and 50 meV photon bandwidth. See text for discussion of the observed features.

B. Emission spectra of NeKr

After confirmation of the Ne dimer ion formation prior to RCT in heterogeneous clusters, we move on to investigate the influence of cluster stoichiometry on the resulting photon spectrum. Three photon spectra emitted from heterogeneous NeKr clusters excited by 23.4 eV photons are shown in Fig. 2. We emphasize that no reliable procedure is known for how to estimate the stoichiometry of heterogeneous clusters from the expansion conditions, i.e., the mean cluster size and mean ratio of the numbers of Ne atoms to Kr atoms in the present case. From semiempirical scaling laws [19,26] and our own previous experiments [27] it is evident that in general the mean cluster size decreases with increasing nozzle temperature and decreasing reservoir pressure. We, therefore, only know that the cluster size decreases from Fig. 2(a) to Fig. 2(c). As the binding energy of Ne atoms in a Ne cluster is much lower than that of Kr atoms in a Kr cluster [28], we further assume that the ratio of condensed Ne to condensed Kr will be lower for higher nozzle temperatures. Consequently, the amount of small clusters, dimers, and monomers increases, and the ratio of condensed Ne compared to condensed Kr decreases from Fig. 2(a) to 2(c).

Five different emission features are observed, which are discussed in the following. The spectrum shown in Fig. 2(a)

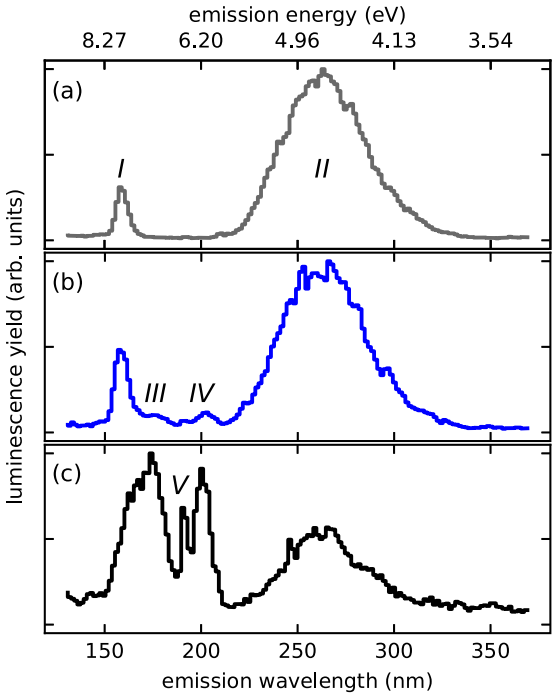

FIG. 2. Dispersed emission spectra of heterogeneous NeKr clusters with different mean sizes and stoichiometries for an exciting-photon energy of 23.4 eV. The spectrum in (a) is identical with the one published earlier (Ref. [10]). In (b) and (c), only the new emerging features are labeled. For individual expansion conditions, see Table I.

has already been published [10] and shows two prominent features I and II. Feature I around 159 nm has been attributed to photon emission from Kr excimers in neutral or ionic clusters [29], or Kr_4^+ [30], following the results of investigations using electron bombardment. The lowest ionization potential of Kr I $4s^2 4p^6$ lies between 11.9 eV for solid Kr and 14.0 eV for the atom [31]. The $4p$ ionization potential of Kr clusters is in between these values and depends on the cluster size: for large clusters values of about 12.25 eV and for small clusters about 12.88 eV have been reported [31]. At an excitation energy of 23.4 eV, photoelectrons with kinetic energy of approximately 11.1 eV are released. This kinetic energy is enough to excite different excitons in homogeneous Kr clusters between 9.95 eV and 10.3 eV via electron scattering [32–34] and explains the appearance of feature I.

Feature II in Fig. 2(a) corresponds to RCT of a Kr $4p$ electron to Ne_2^+, which formed prior to the RCT after the photoionization of a Ne atom. In our previous work, the photon emission was unambiguously correlated to $2p$ ionization of condensed Ne by electron-photon coincidence spectroscopy [10].

The spectrum in Fig. 2(b) originates from a cluster jet with smaller mean cluster size [compared to Fig. 2(a)] and lower Ne content in the clusters. Two weak new features, labeled III and IV, appear. A further decrease in mean cluster size and amount of condensed Ne results in the spectrum shown in Fig. 2(c). Now, features III and IV have grown significantly compared to feature II and an additional feature V is observed.

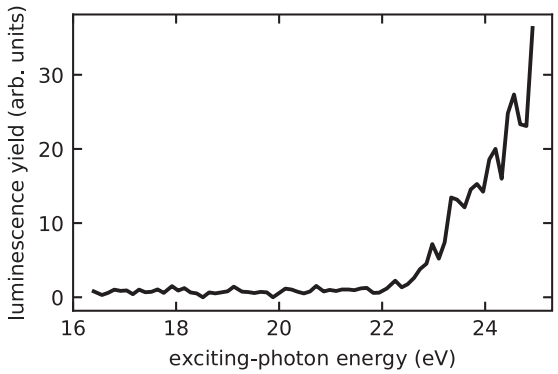

FIG. 3. Emission function of feature I across the Ne $2p$ ionization threshold.

C. Dispersed emission functions of NeKr

To identify the origin of the different features, dispersed photon spectra were measured while varying the exciting-photon energy stepwise across the Ne $2p$ edge. The integrated intensity of the individual features ("emission function") is then plotted versus the exciting-photon energy. The origin of each feature can then be deduced from the onset of the emission function, i.e., the exciting-photon energy at which the signal intensity rises above noise level. Most importantly, all features corresponding to RCT will have their onset slightly below the atomic Ne $2p$ threshold because of the shifted ionization energy in clusters. Additionally, the shift will be larger for larger Ne clusters. Hence the change in clustering conditions can be checked by small changes in the onset value.

The emission function corresponding to feature I is shown in Fig. 3. Its onset appears at about 22.3 eV. This observation strongly supports our earlier interpretation of I as emission from homogeneous Kr aggregates after excitation via photoelectron impact excitation. The photoelectron impact excitation has its onset when the photoelectron kinetic energy is just enough to excite the lowest exciton, which is 9.95 eV + 12.25 eV = 22.2 eV for Kr.

Two emission functions of feature II are shown in Fig. 4(a), comparing the intensity of feature II for medium-sized [solid line, conditions as for the spectrum in Fig. 2(b)] and small clusters [dashed line, conditions as for the spectrum in Fig. 2(c)]. The onset of photon emission by RCT for clusters is between 20.5 eV and 21 eV, matching well our previous observation [10]. The threshold of $2p$ photoionization in clusters is redshifted compared to the monomer. Going from larger to smaller clusters, the onset is slightly less redshifted to exciting-photon energies around 21.0 eV. The different onset of RCT can be explained by the ionization potentials of differently sized clusters: ionization energies for large clusters converge to the value for solid Ne at 20.3 eV [25]. For very small clusters, i.e., composed of only a few atoms, the ionization energy should be near the ionization limit of atoms at 21.56 eV [10]. This observation thus confirms that the clusters in spectrum Fig. 2(c) are indeed somewhat smaller than in Fig. 2(a). The shape of feature II does not change qualitatively for the different expansion conditions. We conclude that this kind of RCT is not influenced by the exact cluster size or stoichiometry, as long as enough Ne is present to form Ne_2^+.

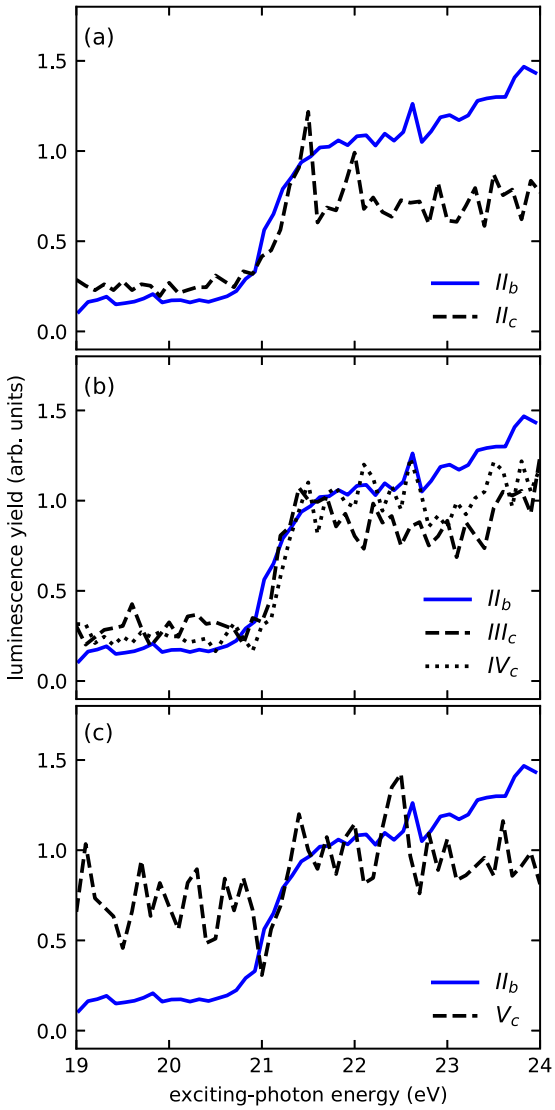

FIG. 4. Emission functions between 19 eV and 24 eV of the observed features as spectrally assigned in Fig. 2. The individual curves are labeled according to the respective feature and the subscript indicating the expansion conditions (see Table I). (a) Feature II for large (IIb, solid line) and small (IIc, dashed line) clusters. (b) Features III (dashed line) and IV (dotted line) for small clusters. (c) Feature V (dashed line) for small clusters. For comparison, the emission function IIb is shown in all panels.

The emission function of feature III is shown in Fig. 4(b). For comparison, also the emission function of RCT in large clusters (feature II) is shown in the same panel. The onset of III is at about 21 eV, suggesting its origin to be RCT, just like feature II for small clusters.

Indeed, the emission band III around 174 nm in Figs. 2(b) and 2(c) can be assigned to photon emission originating from an electron transfer in an ionized NeKr dimer, which had already been reported from high-pressure gas cell experiments using discharges as the excitation source [15]. The broad emission consists of contributions from different vibrational states which are not well resolved in the present experiment, from approximately 162 nm to 183 nm. Vibrational structures are often not observable in clusters above a certain size, because the vibrational energy dissipates and leads to evaporation of atoms [35]. The photon emission for different vibrational states of RCT in ionized NeKr dimers is also well explained by theory [14].

The occurrence of dimers can be explained by two contributions. The first one is the direct creation of dimers due to the chosen expansion conditions. The conditions support the formation of relatively small clusters; therefore, a significant amount of NeKr dimers should appear in the target although it cannot be quantified. Second, vibrationally excited ionized clusters may relax via the redistribution of vibrational energy, finally leading to the evaporation of atoms [35]. Since the binding energy of noble gas clusters is typically very weak, vibrational relaxation may easily evaporate large numbers of atoms and lead to the formation of ionized $NeKr^+$ dimers from small clusters. If the vibrational energy is larger than the binding energies of all neighboring atoms, the excited cluster cannot relax into the vibrational ground state by desorption of atoms, which is the reason for the width of feature III.

The emission function of feature IV is also shown in Fig. 4(b) (dotted line). The feature is located around 201 nm, with a width of approximately 8 nm. Within the experimental statistics, the emission function is identical to those of features II and III for small clusters. The appearance of feature IV can therefore unambiguously be attributed to the ionization of condensed Ne. No emission from homogeneous Ne or Kr nor from heterogeneous NeKr clusters other than RCT is known to have its onset at the $2p$ ionization threshold of condensed Ne. Compared with features I and III, however, feature IV apparently can neither be attributed to the formation of Ne_2^+ in large clusters nor to emission from NeKr dimers. The origin of this feature cannot be identified unambiguously with the present data. Its appearance at shorter wavelengths in the spectrum suggests that it represents RCT from Kr to Ne_2^+ dimers which are not in the $^2\sigma_u^+$ ground state (see Ref. [10]). It remains, however, unclear why the feature only appears in the spectrum of relatively small clusters.

Finally, the emission function of feature V around 191 nm is shown in Fig. 4(c) and compared to feature II. The intensity of feature V does not vary with changing exciting-photon energy in the investigated energy range. Combining the information from the emission spectrum and the emission function, feature V cannot be attributed to any emission from condensed Ne or Kr. Its independence of exciting-photon energy suggests that it originates from higher-order radiation of the synchrotron beamline, e.g., from the radiative decay of photoelectron satellite states in Ne atoms. The population of photoelectron satellite states of Ne $2p^4nl$ character with $n \geqslant 3$ and $l = s,\ p$, and d is well investigated [36,37]. Optical transitions from ns and nd orbitals to the Ne II $2s^22p^5$ ground state correspond to wavelengths below 50 nm and cannot be detected in the present experiment [20]. Due to dipole selection rules, Rydberg states with np character decay via fluorescence cascades. The $2p^43p$ photoelectron satellite states decay by optical transitions to intermediate $2p^43s$ states between 187 nm and 194 nm. These wavelengths fit well to the observed feature V and therefore we assume that the observed emission originates from optical decays of photoelectron satellite states.

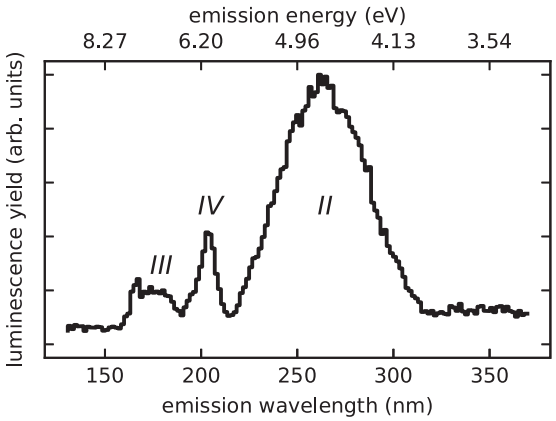

FIG. 5. Dispersed emission spectrum of small NeKr clusters at an exciting-photon energy of 21.9 eV, measured at the U125-2-NIM beamline.

Features I and III overlap in emission wavelengths as can be seen by comparing Figs. 2(a) to 2(c). As a cross-check of the observed RCT emissions, an emission spectrum with excitation energy of 21.9 eV is shown in Fig. 5, measured in a separate experiment (see Experiments section). At this exciting-photon energy the kinetic energy of the created photoelectrons is not large enough to excite Kr excitons and therefore feature I is absent. The emission ranges from 160 nm to 188 nm, which, except for a slight shift of the high-wavelength cutoff, agrees well with the observation of Ref. [15]. Under the experimental conditions of Ref. [15], only dimer formation is expected; thus our interpretation agrees well with the observation. In Table II, we provide an overview of the observed features and their assignments based on the present data.

D. Lifetimes

Following the observations of the preceding sections, it is an intriguing question whether further properties of the RCT process are influenced by the cluster stoichiometry. Besides the photon spectrum, another characteristic property of radiative decays is the lifetime of the decaying state. To estimate whether the lifetime will be affected by the stoichiometry, we performed calculations of the decay widths for different local arrangements of the involved atoms. The decay width is directly connected to the lifetime of the RCT initial state, which is an accessible experimental observable. Our calculations predict RCT lifetimes in $NeKr^+$ dimers, $Ne_2{}^+Kr$ trimers, and $Ne_2{}^+Kr_2$ tetramers in the order of nanoseconds. As expected,

TABLE II. Overview of the assignments of the different observed features in the photon spectra.

Feature	Assignment
I	Electron impact excitation of Kr
II	RCT in large clusters ($Ne_2{}^+$ formation)
III	RCT in small clusters ($NeKr^+$ formation)
IV	RCT in small clusters
V	Ne monomer photoelectron satellites

TABLE III. RCT lifetimes obtained for two different expansion temperatures. All other experimental parameters were kept constant, e.g., the mixing ratio in the gas reservoir, which was 98.8 % Ne and 1.2 % Kr. For more experimental details, see Ref. [10].

T (K)	τ (ns)
93.5	70 ± 1
87.0	82 ± 1

the lifetimes are sensitive to the explicit local arrangement and the internuclear distances. As a very general result, we observe that the RCT lifetime in $NeKr^+$ dimers is considerably shorter than in the case when $Ne_2{}^+$ forms and an electron is transferred from an adjacent Kr atom to the dimer ion.

To our knowledge, no experimental values of lifetimes of this type of RCT have been reported yet. As a proof of principle, that the RCT lifetime critically depends on the cluster production parameters, we reanalyzed our earlier experiment on RCT in single bunch mode with respect to time resolved photon detection [10]. The lifetimes are obtained by measuring the detection time of each individual photon event with respect to the exciting synchrotron radiation pulse and fitting an exponential decay to the histogram of these values (see Ref. [17] for details). Only photons in coincidence with Ne cluster $2p$ photoelectrons were considered, thus eliminating possible radiative processes other than RCT. Since the photons are not detected spectrally resolved in this experiment (see Sec. II), the lifetime values are averages over all cluster sizes and stoichiometries.

Also in this experiment, the target preparation does not allow one to select specific cluster sizes or stoichiometries, but averages over a wide distribution. By changing the expansion parameters, however, the average target properties can be varied to obtain clusters of smaller or larger mean size and containing different amounts of Ne. Two lifetime measurements were performed, the parameters of which are shown in Table III. The experimental data is well fitted by a single exponential decay. It may, however, in fact be the result of a large number of individual decay functions with different lifetimes, corresponding to RCT for different local arrangements, which cannot be disentangled. The obtained values thus do not represent the change in lifetime of a single decay, but rather give information about the statistical importance of arrangements with shorter or longer lifetime.

We observe a significant increase in average RCT lifetime for lower nozzle temperature, which is in agreement with our calculations. As the nozzle temperature decreases, more Ne will condense within the clusters and the contribution of RCT in $NeKr^+$ dimers will become smaller, thus increasing the average observable lifetime.

In order to understand theoretically how the lifetime of the RCT process changes with cluster size and stoichiometry, we considered three clusters: the $NeKr^+$ dimer, the $Ne_2{}^+Kr$ trimer, and the $Ne_2{}^+Kr_2$ tetramer. In the case of the trimer and tetramer, the two Ne atoms were kept at a distance of 1.7 Å apart, which is a result of $Ne_2{}^+$ formation prior to the RCT process (see Ref. [10]). The geometries of the three types of clusters are shown in Fig. 6.

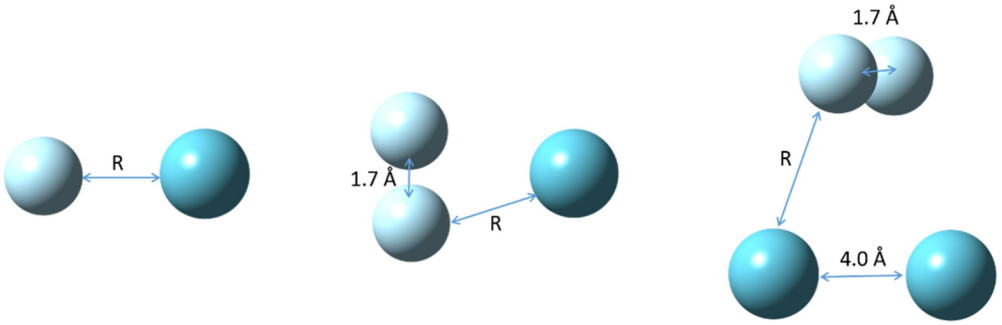

FIG. 6. Local atomic arrangements of three types of NeKr clusters—$NeKr^+$ (left), $Ne_2{}^+Kr$ (middle), and $Ne_2{}^+Kr_2$ (right). The distance between the Ne atoms in the case of the trimer and tetramer was fixed to 1.7 Å, whereas the distance between the two Kr atoms in the tetramer was fixed to 4.0 Å.

The energies and transition dipole moments used to compute the RCT lifetime were calculated with the multireference configuration interaction (MRCI) method [38–40] as implemented in the MOLPRO computational package [41,42]. The aug-cc-pVDZ basis set [43,44] was used on both atoms in the case of the trimer and tetramer, whereas in the case of the dimer the aug-cc-pV5Z basis set was employed [43,44]. The calculated RCT lifetimes for the initial RCT states $Ne_n{}^+Kr_m$ (where $n, m = 1, 2$) for the three clusters studied are shown in Tables IV, V, and VI. The last column of all tables shows the total lifetime for a given initial state. It was computed as the inverse of the total decay width Γ, which is a sum of the partial decay widths Γ_i to all possible final states

$$\tau = \frac{\hbar}{\Gamma}, \quad \Gamma = \sum_{i=1}^{n} \Gamma_i. \tag{1}$$

For all three clusters, the RCT lifetime was computed for various distances between Ne and Kr. In general, the lifetime increases with the distance. This is a result of the decreasing overlap between the initial and final states.

The case of the dimer can easily be understood. The transition between $Ne^+Kr\ \Sigma^+$ and $NeKr^+\ \Sigma^+$ states has the shortest RCT lifetime of 7 ns at 3.3 Å (see Table IV). The Ne^+Kr and $NeKr^+\ \Sigma^+$ states can be described with a main configuration where the hole is in the Ne $2p_z$ and Kr $4p_z$ orbitals, respectively (where z is the interatomic axis). Since these orbitals are oriented on the interatomic axis, the overlap between them is large, which then results in a larger transition dipole moment and a shorter RCT lifetime for the $\Sigma^+ \rightarrow \Sigma^+$ RCT transition.

The shortest RCT lifetimes for the trimer and tetramer are 86 ns and 66 ns, thus being longer than the shortest RCT lifetimes of the dimer. This result can be rationalized based on the poorer overlap between the initial and final RCT states in the trimer and tetramer. The lifetimes of the initial $Ne_2{}^+Kr$ states of the trimer are longer compared to the tetramer most probably due to the increased number of neighbors, and thus decay channels through which RCT can occur.

The theoretical values are in an overall very good agreement with the experimental ones. The differences can be attributed to the fact that the experimental lifetime is an average value over a distribution of cluster sizes, stoichiometries, and local geometries, whereas the computed lifetimes are for a single atomic arrangement. Moreover, the nuclear motion following ionization is not accounted for in the theoretical calculation. If the distance between the Ne dimer ion and Kr decreases, one should expect a faster RCT.

TABLE IV. RCT lifetimes for the $NeKr^+$ dimer. The lifetimes are presented at the equilibrium distance of the (neutral) NeKr dimer (R_{eq} = 3.7 Å [45]) and at the distance corresponding to the minimum of the potential-energy curve [$R(E_{min})$ = 3.3 Å for $Ne^+Kr\ \Sigma^+$ state; $R(E_{min})$ = 3.2 Å for $Ne^+Kr\ \Pi$ state]. The last column shows the total lifetime for a given initial Ne^+Kr state.

RCT transition				
Ne^+Kr	$NeKr^+$	τ (ns) at R_{eq}	τ (ns) at $R(E_{min})$	τ_{tot} (ns)
Σ^+	Σ^+	24	7 (3.3 Å)	24 (3.7 Å)/ 7 (3.3 Å)
Σ^+	Π	4.9×10^5	1.92×10^5	
Π	Σ^+	4623	1193 (3.2 Å)	1146 (3.7 Å)/ 196 (3.2 Å)
Π	Π	1524	234	

TABLE V. RCT lifetimes for the singly ionized $Ne_2{}^+Kr$ trimer. The lifetimes are presented at a distance of 3.7 Å between Ne and Kr, which corresponds to the equilibrium distance of the dimer [45].

$Ne_2{}^+Kr$ initial state	τ_{tot} (ns)
$2A_1$	86
$3A_1$	4198
$2B_1$	4008
$2B_2$	2.3×10^4
$3B_2$	944
$1A_2$	1.3×10^5

IV. CONCLUSION

We present a systematic study of radiative charge transfer (RCT) in heterogeneous noble clusters using the photon emission of NeKr clusters after Ne $2p$ photoionization. Notwithstanding the lack of a model to accurately determine the size and stoichiometry of the heterogeneous clusters, we

TABLE VI. RCT lifetimes for the singly ionized $Ne_2{}^+Kr_2$ tetramer. The lifetimes are presented at a distance of 3.7 Å between Ne and Kr, which corresponds to the equilibrium distance of the dimer [45].

$Ne_2{}^+Kr_2$ initial state	τ_{tot} (ns)
$2A_2$	1575
$2B_1$	1.3×10^4
$3B_1$	720
$3B_2$	142
$3A_1$	66
$4A_1$	2142

observe pronounced changes in the photon spectra as a function of the cluster production parameters. The results are in line with considerations on the mean cluster size and stoichiometry for the different conditions. For large clusters and high Ne concentration, the photon spectrum is dominated by the emission corresponding to charge transfer from Kr to $Ne_2{}^+$, which forms after photoionization. For less Ne and smaller clusters, other features emerge and finally take over, which can be attributed to RCT in NeKr dimers. We conclude that, under these conditions, the amount of Ne is too low to enable $Ne_2{}^+$ formation prior to RCT.

Theoretical calculations revealed that the RCT decay width crucially depends on the nature of the charge transfer and the local arrangement of the involved atoms. We confirmed this fact experimentally by determining the average lifetimes corresponding to the radiative decay for two different cluster conditions. In agreement with the theoretical prediction, the lifetime increases for larger clusters and higher Ne concentration.

We propose that the properties of RCT may be utilized in general to characterize the size, stoichiometry, and dynamics of heterogeneous cluster jets and hope that our results may stimulate further effort to develop more accurate models on the cluster formation.

ACKNOWLEDGMENTS

The work was partially supported by a grant from the Otto-Braun-Fonds (Melsungen). We acknowledge HZB for beamtime allocation and the BESSY II staff for support during the experiments. This work was funded by the Deutsche Forschungsgemeinschaft (DFG, German Research Foundation) through research unit FOR 1789 and the German Federal Ministry of Education and Research through Project No. 05K19RK2.

[1] L. S. Cederbaum, J. Zobeley, and F. Tarantelli, Phys. Rev. Lett. **79**, 4778 (1997).
[2] U. Hergenhahn, J. Electron Spectrosc. Relat. Phenom. **184**, 78 (2011).
[3] T. Jahnke, J. Phys. B: At., Mol., Opt. Phys. **48**, 082001 (2015).
[4] T. Jahnke, U. Hergenhahn, B. Winter, R. Dörner, U. Frühling, P. V. Demekhin, K. Gokhberg, L. S. Cederbaum, A. Ehresmann, A. Knie, and A. Dreuw, Chem. Rev. **120**, 11295 (2020).
[5] T. Arion and U. Hergenhahn, J. Electron Spectrosc. Relat. Phenom. **200**, 222 (2015).
[6] J. Voigtsberger, S. Zeller, J. Becht, N. Neumann, F. Sturm, H.-K. Kim, M. Waitz, F. Trinter, M. Kunitski, A. Kalinin, J. Wu, W. Schöllkopf, D. Bressanini, A. Czasch, J. B. Williams, K. Ullmann-Pfleger, L. P. H. Schmidt, M. S. Schöffler, R. E. Grisenti, T. Jahnke *et al.*, Nat. Commun. **5**, 5765 (2014).
[7] J. Jortner, Z. Phys. D **24**, 247 (1992).
[8] C.-R. Wang, R.-B. Huang, Z.-Y. Liu, and L.-S. Zheng, Chem. Phys. Lett. **227**, 103 (1994).
[9] R. von Pietrowski, K. von Haeften, T. Laarmann, T. Möller, L. Museur, and A. V. Kanaev, Eur. Phys. J. D **38**, 323 (2006).
[10] A. Hans, T. Miteva, X. Holzapfel, C. Ozga, P. Schmidt, H. Otto, G. Hartmann, C. Richter, N. Sisourat, A. Ehresmann, K. Gokhberg, U. Hergenhahn, and A. Knie, Phys. Rev. Lett. **123**, 213001 (2019).
[11] N. Saito, Y. Morishita, I. H. Suzuki, S. D. Stoychev, A. I. Kuleff, L. S. Cederbaum, X.-J. Liu, H. Fukuzawa, G. Prümper, and K. Ueda, Chem. Phys. Lett. **441**, 16 (2007).
[12] I. Higuchi, T. Ouchi, K. Sakai, H. Fukuzawa, X.-J. Liu, K. Ueda, H. Iwayama, K. Nagaya, M. Yao, D. Ding, D. Zhang, Y. Tamenori, and N. Saito, J. Phys.: Conf. Ser. **235**, 012015 (2010).
[13] A. Hans, V. Stumpf, X. Holzapfel, F. Wiegandt, P. Schmidt, C. Ozga, P. Reiß, L. B. Ltaief, C. Küstner-Wetekam, T. Jahnke, A. Ehresmann, P. V. Demekhin, K. Gokhberg, and A. Knie, New J. Phys. **20**, 012001 (2018).
[14] D. Hausamann and H. Morgner, Mol. Phys. **54**, 1085 (1985).
[15] Y. Tanaka, K. Yoshino, and D. E. Freeman, J. Chem. Phys. **62**, 4484 (1975).
[16] G. Reichardt, J. Bahrdt, J.-S. Schmidt, W. Gudat, A. Ehresmann, R. Müller-Albrecht, H. Molter, H. Schmoranzer, M. Martins, N. Schwentner, and S. Sasaki, Nucl. Instrum. Methods Phys. Res., Sect. A **467**, 462 (2001).
[17] A. Hans, P. Schmidt, C. Ozga, G. Hartmann, X. Holzapfel, A. Ehresmann, and A. Knie, Materials **11**, 869 (2018).
[18] V. Sukhorukov, I. Petrov, B. Lagutin, A. Ehresmann, K.-H. Schartner, and H. Schmoranzer, Phys. Rep. **786**, 1 (2019).
[19] U. Buck and R. Krohne, J. Chem. Phys. **105**, 5408 (1996).
[20] A. Kramida, Y. Ralchenko, J. Reader, and NIST ASD Team, available at https://physics.nist.gov/asd, National Institute of Standards and Technology, Gaithersburg, MD, 2020.
[21] A. Knie, A. Hans, M. Förstel, U. Hergenhahn, P. Schmidt, P. Reiß, C. Ozga, B. Kambs, F. Trinter, J. Voigtsberger, D. Metz, T. Jahnke, R. Dörner, A. I. Kuleff, L. S. Cederbaum, P. V. Demekhin, and A. Ehresmann, New J. Phys. **16**, 102002 (2014).
[22] A. Hans, A. Knie, M. Förstel, P. Schmidt, P. Reiß, C. Ozga, U. Hergenhahn, and A. Ehresmann, J. Phys. B **49**, 105101 (2016).
[23] I. Fugol', O. N. Grigorashchenko, A. N. Ogurtsov, and E. V. Savchenko, J. Lumin. **53**, 517 (1992).
[24] E. A. Bondarenko, E. T. Verkhovtseva, Y. S. Doronin, and A. M. Ratner, Chem. Phys. Lett. **182**, 637 (1991).
[25] N. Schwentner, E.-E. Koch, and J. Jortner, *Electronic Excitations in Condensed Rare Gases*, Springer Tracts in Modern Physics Vol. 107 (Springer, Berlin, 1985).
[26] O. F. Hagena and W. Obert, J. Chem. Phys. **56**, 1793 (1972).

[27] X. Holzapfel, A. Schrodt, G. Hartmann, L. Marder, P. Schmidt, C. Ozga, P. Reiß, F. Wiegandt, A. Ehresmann, A. Hans, and A. Knie, J. Phys. Chem. A **124**, 5352 (2020).
[28] T. Arion, M. Mucke, M. Förstel, A. M. Bradshaw, and U. Hergenhahn, J. Chem. Phys. **134**, 074306 (2011).
[29] É. T. Verkhovtseva, E. A. Bondarenko, and Y. S. Doronin, Low Temp. Phys. **30**, 34 (2004).
[30] Y. S. Doronin, V. N. Samovarov, and E. A. Bondarenko, Low Temp. Phys. **32**, 251 (2006).
[31] G. Ganteför, G. Bröker, E. Holub-Krappe, and A. Ding, J. Chem. Phys. **91**, 7972 (1989).
[32] J. Stapelfeldt, J. Wörmer, G. Zimmerer, and T. Möller, Z. Phys. D - Atoms, Molecules and Clusters **12**, 435 (1989).
[33] T. Möller, Z. Phys. D - Atoms, Molecules and Clusters **20**, 1 (1991).
[34] L. B. Ltaief, A. Hans, P. Schmidt, X. Holzapfel, F. Wiegandt, P. Reiß, C. Küstner-Wetekam, T. Jahnke, R. Dörner, A. Knie, and A. Ehresmann, J. Phys. B: At., Mol., Opt. Phys. **51**, 065002 (2018).
[35] R. Karnbach, M. C. Castex, J. W. Keto, M. Joppien, J. Wörmer, G. Zimmerer, and T. Möller, Chem. Phys. Lett. **203**, 248 (1993).
[36] P. A. Heimann, U. Becker, H. G. Kerkhoff, B. Langer, D. Szostak, R. Wehlitz, D. W. Lindle, T. A. Ferrett, and D. A. Shirley, Phys. Rev. A **34**, 3782 (1986).
[37] B. Zimmermann, K. H. Schartner, O. Wilhelmi, S. Kammer, H. Liebel, A. Ehresmann, and H. Schmoranzer, J. Phys. B **37**, 511 (2004).
[38] H.-J. Werner and P. J. Knowles, J. Chem. Phys. **89**, 5803 (1988).
[39] P. J. Knowles and H.-J. Werner, Chem. Phys. Lett. **145**, 514 (1988).
[40] K. R. Shamasundar, G. Knizia, and H.-J. Werner, J. Chem. Phys. **135**, 054101 (2011).
[41] H.-J. Werner, P. J. Knowles, G. Knizia, F. R. Manby, and M. Schütz, Wiley Interdiscip. Rev.: Comput. Mol. Sci. **2**, 242 (2012).
[42] H.-J. Werner, P. J. Knowles, G. Knizia, F. R. Manby, M. Schütz, P. Celani, W. Györffy, D. Kats, T. Korona, R. Lindh, A. Mitrushenkov, G. Rauhut, K. R. Shamasundar, T. B. Adler, R. D. Amos, S. J. Bennie, A. Bernhardsson, A. Berning, D. L. Cooper, M. J. O. Deegan *et al.*, MOLPRO, version 2012.1, a package of *ab initio* programs, 2012.
[43] T. H. Dunning, J. Chem. Phys. **90**, 1007 (1989).
[44] A. K. Wilson, D. E. Woon, K. A. Peterson, and T. H. Dunning, J. Chem. Phys. **110**, 7667 (1999).
[45] R. Candori, F. Pirani, and F. Vecchiocattivi, Mol. Phys. **49**, 551 (1983).